

Nanoscale

Accepted Manuscript



This is an *Accepted Manuscript*, which has been through the Royal Society of Chemistry peer review process and has been accepted for publication.

Accepted Manuscripts are published online shortly after acceptance, before technical editing, formatting and proof reading. Using this free service, authors can make their results available to the community, in citable form, before we publish the edited article. We will replace this *Accepted Manuscript* with the edited and formatted *Advance Article* as soon as it is available.

You can find more information about *Accepted Manuscripts* in the [Information for Authors](#).

Please note that technical editing may introduce minor changes to the text and/or graphics, which may alter content. The journal's standard [Terms & Conditions](#) and the [Ethical guidelines](#) still apply. In no event shall the Royal Society of Chemistry be held responsible for any errors or omissions in this *Accepted Manuscript* or any consequences arising from the use of any information it contains.



Journal Name

ARTICLE

Self-supported Zn₃P₂ Nanowires Arrays Grafted on Carbon Fabrics as an Advanced Integrated Anode for Flexible Lithium Ion Battery

Wenwu Li,^a Lin Gan,^a Kai Guo,^a Linbo Ke,^a Yaqing Wei,^a Huiqiao Li,^a Guozhen Shen^{*b} and Tianyou Zhai^{*a}

Received 00th January 20xx,
Accepted 00th January 20xx

DOI: 10.1039/x0xx00000x

www.rsc.org/

We, for the first time, successfully graft well-aligned binary lithium-reactive zinc phosphide (Zn₃P₂) nanowires arrays on carbon fabrics cloth by a facile CVD method. When served as a novel self-supported binder-free anode for lithium ion batteries (LIBs), the hierarchical three-dimension (3D) integrated anode shows excellent electrochemical performances: a highly reversible initial lithium storage capacity of ca. 1200 mA h g⁻¹ with a coulombic efficiency up to 88%, long lifespan of over 200 cycles without obvious decay, and high rate capability of ca. 400 mA h g⁻¹ capacity retention at an ultrahigh rate of 15 A g⁻¹. More interestingly, a flexible LIB full cell is assembled on the basis of the as-synthesized integrated anode and commercial LiFePO₄ cathode, which shows striking lithium storage performances very close to the half cells: a large reversible capacity over 1000 mA h g⁻¹, a long-cycle life over 200 cycles without obvious decay, and an ultrahigh rate performance with ca. 300 mA h g⁻¹ even at 20 A g⁻¹. Considering the excellent lithium storage performances of coin-type half cells as well as flexible full cells, the as-prepared carbon cloth grafted well-aligned Zn₃P₂ nanowires arrays would be a promising integrated anode for flexible LIB full cell devices.

Introduction

In view of the fast growing demands in energy storage devices, especially for flexible and wearable electronic applications, the research on foldable energy storage batteries is of great significance.¹⁻⁵ Till now, rechargeable lithium-ion batteries (LIBs) is one of the most widely used energy-storage devices due to their extraordinary inherent characteristics: high energy density, high operating voltage, long cycling lifespan, and environmentally friendly products et al.⁶⁻⁸ The central point for flexible full cells assembling is to develop flexible integrated electrodes with highly reversible lithium storage capacity. Among the most reported anode materials for flexible full cells, nanostructured carbon-based materials⁹ have attracted considerable attention due to their high electric conductivities, as well as metal oxides¹⁰⁻¹⁴ due to their large capacities. However, the low capacities of carbon-based materials limit the energy density of the bendable full cells. Similarly, the low electric conductivities of metal oxides degrade the initial coulombic efficiency and rate capability of the full cell devices. Although many efforts have been devoted to combine the

merits of the two kinds of materials,¹²⁻¹⁴ the progress is still far from satisfactory. Therefore, there are still full of great challenges to explore new kinds of integrated anodes with large capacity, long-cycle life, high-rate, as well as high energy and power densities for flexible LIB full cell device.

Metal phosphides are emerging promising anode materials for rechargeable secondary batteries¹⁵⁻²³ due to their excellent electric conductivity, high capacity and relatively low and flat potential plateaus.²⁴⁻³³ However, they are mainly limited to specific morphology so far, i.e. the form of aggregated nanoparticles acquired by high energy mechanical milling.^{24-27,34-35} The seriously agglomeration of these ball-milled metal phosphide nanoparticles deteriorate the reaction surface area, ions diffusion, and electrolyte soakage of electrode on the one hand and also degrade the conductivity of the whole electrode due to large numbers of boundaries between the nanoparticles on the other hand. Therefore, their cycle and rate performances are severely suppressed. Many efforts have been adopted to resolve the above-mentioned problems, and the widely used strategy is to blend active materials with carbon.³⁴⁻³⁵ Taking ZnP₂ as an example, to some degree, the surface area and conductivity of ZnP₂ electrode can be improved by adding a large quantity of low-capacity carbon (35 wt%) into the whole electrode.³⁴⁻³⁵ Unfortunately, it can only prolong the lifespan slightly, still less than 20 cycles. This can be attributed to such an arbitrary mixing strategy in which active materials blends with carbon without any functional structural design, therefore it is hard to prevent the aggregation of ZnP₂ and ensure a well-distributed composite, in other words, it cannot make full use of the buffer effect and

^a State Key Laboratory of Material Processing and Die & Mould Technology, School of Materials Science and Engineering, Huazhong University of Science and Technology (HUST), Wuhan 430074, Hubei, P. R. China.
E-mail: zhaiy@hust.edu.cn.

^b State Key Laboratory for Superlattices and Microstructures, Institute of Semiconductors, Chinese Academy of Sciences, Beijing 100083, P. R. China.

^c E-mail: gzshen@semi.ac.cn.

Electronic Supplementary Information (ESI) available: [details of any supplementary information available should be included here]. See DOI: 10.1039/x0xx00000x

good conductivity of carbon. Notably, most researchers mainly focus on the coin-type half cells lithium storage performances of phosphides. In contrast, the study of full cells is rare to date, however, which is critical to the evaluation of active materials application potential. Because full cells are the practical application forms but their performances are generally much worse than the performances of coin-type half cells. Therefore, full utilization of the large capacity of active materials in full cells is still full of challenges.

Herein we for the first time synthesized the self-supported Zn_3P_2 nanowires arrays on carbon fabric cloth as an integrated binder-free anode through a facile chemical vapor deposition. This structure design can effectively prevent the agglomeration of Zn_3P_2 occurred in mechanical milling method, provide a large reaction surface, and ensure fast and reliable electronic conductivity. When applied as novel integrated anodes for half cells of LIBs, the as-synthesized materials represent excellent electrochemical performances: a highly reversible initial lithium storage capacity of ca. 1200 mA h g^{-1} with the coulombic efficiency up to 88%, long lifespan of over 200 cycles without obvious decay, and high rate capability of ca. 400 mA h g^{-1} capacity retention at an ultrahigh rate of 15 A g^{-1} . More importantly, superior to most reported anode materials,^{24-26,33-35} this novel anode based full cells can maintain excellent performances pretty close to corresponding half cells, paving the way for its practical applications.

carbon cloth and it can be rolled up periodically with a tweezers.

The growth process is illustrated in **Figure 1a** and the morphologies of the as-grown self-supported binder-free Zn_3P_2 nanowires arrays on carbon fabrics cloth are observed by using field emission scanning electron microscopy (SEM). As shown in **Figure 1b**, generally, the uniform three-dimensional hierarchical integrated electrode is covered densely with Zn_3P_2 nanowires arrays. The low-magnification SEM images shown in **Figure 1b and 1c** represent the contour shape of well-established texture structure with the as-synthesized Zn_3P_2 nanowires arrays grown on all of the carbon fabrics of the carbon cloth, where every carbon fabric fiber (ca. $9 \mu\text{m}$ in original diameter) grew to $17 \mu\text{m}$ in diameter, much larger than that of an uncovered singular carbon fabric microfiber. Furthermore, compared with a singular uncovered carbon fabric microfiber with slightly smooth surfaces, the integrated anode has rough surfaces. The high-magnification SEM images indicated in **Figure 1d and 1e** clearly provide detailed information of the Zn_3P_2 nanowires arrays, where the numerous ultrathin nanowires are found adhered tightly to each carbon fabric microfiber in the radial manner to form a novel three-dimensional hierarchical nanostructured architecture. Such featured integrated anodes can deliver immediate electron transports and good contact between Zn_3P_2 nanowires and the micro-sized carbon fabrics current collector. Therefore, electrons can be transferred as quickly as they could from the lithium-reactive redox sites to the micro-sized carbon fabric current collector along a high-express way without large electrons scatter caused by the particle boundary barriers. Moreover, the wide open spaces between the nanowires arrays can ease electrolyte penetrating into the integrated anode to increase the contact areas between electrolyte and electrode as well as decrease the Li^+ diffusion length. The large volume change and the severe aggregation of Zn and P in the electrode-reaction products during charge/discharge processes can also be accommodated well by the wide open spaces and loose textures of the carbon microfibers. And these merits of the array structure can be presented in the lithium diffusion model (**Figure 4**). Compared to other current collectors, carbon textures possess higher conductivity, better flexibility, and higher stability in corrosive organic electrolyte.³⁶⁻⁴¹

Results and discussion

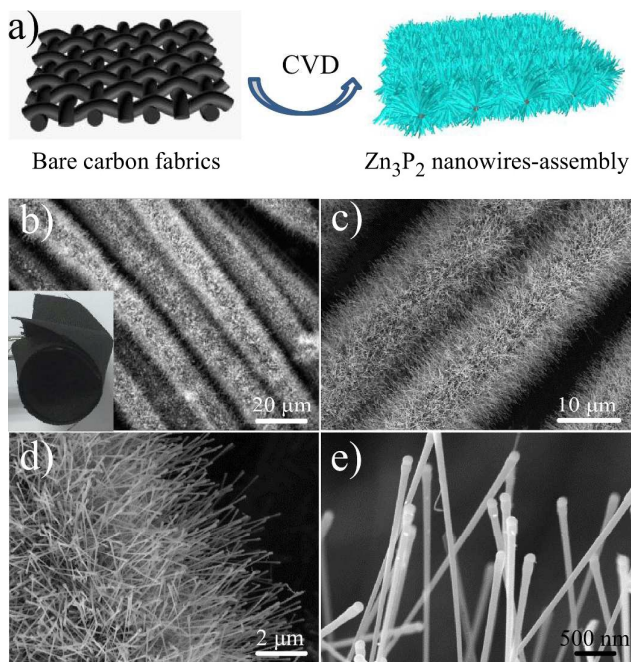


Figure 1. (a) Schematic illustration of the preparation of flexible three-dimensional Zn_3P_2 nanowire arrays/carbon cloth. Morphology characterization: (b-e) Typical SEM images of the Zn_3P_2 nanowire arrays grown on carbon cloth at different magnifications. Inset in panel b: Photographic image of flexible

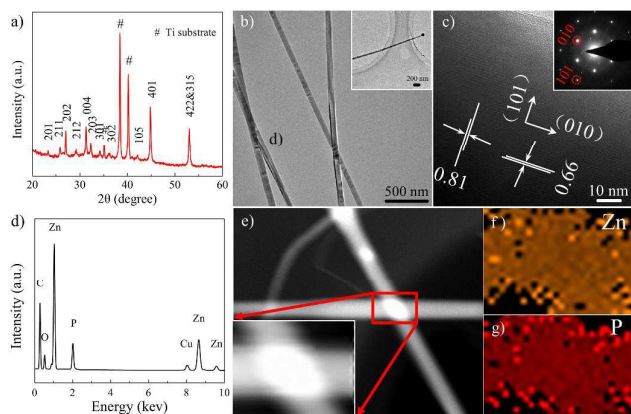


Figure 2. Phase analysis. (a) XRD pattern of Zn_3P_2 . (b-c) TEM and high-resolution TEM images of hierarchical Zn_3P_2 nanowire. (d) The EDS microanalysis of the Zn_3P_2 nanowires. (e) SEM image and the corresponding selected area elemental mappings: (f) Zn and (g) P.

Pure phase of the as-prepared integrated anode is confirmed by the X-ray diffraction result as shown in **Figure 2a**. All of the fingerprint diffraction peaks, except for that of the substrate, can be readily assigned to pure Zn_3P_2 with a tetragonal phase of Zn_3P_2 (JCPDS Card No. 74-1156; $a = 8.097 \text{ \AA}$; $c = 11.450 \text{ \AA}$). To observe more specific microstructure of the as-grafted Zn_3P_2 nanowires, transmission electron microscope (TEM) as well as high-resolution transmission electron microscope (HRTEM) characterizations were carried out. At low magnification, as shown in **Figure 2b**, these obtained upright Zn_3P_2 nanowires possess an average diameter of approximate 80 nm and a length up to several micrometers. Au nanoparticles can be clearly found adhered to the tips of the grown nanowires, as shown in the inset of **Figure 2b**, confirming the growth of nanowires undergoes a typical vapour liquid solid (VLS) process. The composition of the typical nanowires were investigated by energy dispersive spectrometer (EDS) and elemental mapping in the scanning transmission electron microscopy (STEM). As shown in **Figure 2d**, the signals from both Zn and P of the spectrum are from Zn_3P_2 and no other impurities can be found. The elemental mapping (**Figure 2e-2g**) of the marked region by red rectangle (**Figure 2e**) also shows Zn and P elements are highly homogeneously distributed in molar ratio of 3 to 2. A typical HRTEM image of a typical individual Zn_3P_2 nanowire is represented in **Figure 2c**. The well-defined lattice fringes are measured to be 0.66 nm perpendicular to as well as 0.81 nm along its longitudinal axis of Zn_3P_2 nanowire, respectively, in consistent with the (101) and (010) planes of the tetragonal Zn_3P_2 . Besides, the corresponding selected area electron diffraction (SAED) pattern of an individual Zn_3P_2 nanowire is also shown in the inset of **Figure 2c**, demonstrating the single crystalline feature of the nanowire. Together with the HRTEM result, it can be concluded that the growth direction of typical Zn_3P_2 nanowire is along the [010] crystallographic orientation.

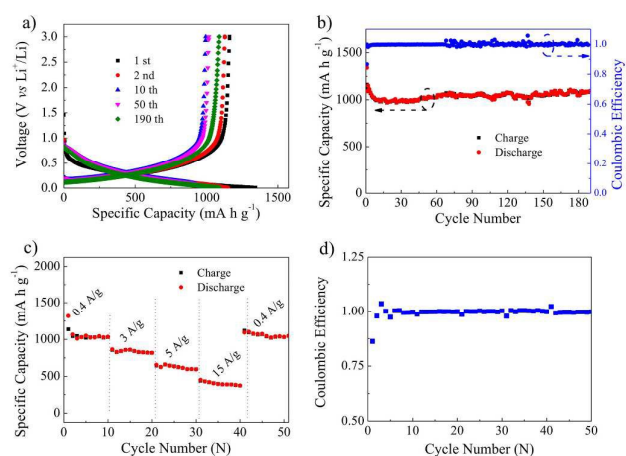


Figure 3. Electrochemical characterizations: (a) the voltage vs. specific capacity profiles for the 1st, 2nd, 10th, 50th and 190th discharge and charge cycle. (b) Long-term cycling of the Zn_3P_2 nanowire arrays/carbon cloth electrode. (c) The rate performances of the Zn_3P_2 nanowire arrays/carbon cloth electrode. (d) The corresponding coulombic efficiency curves at different rates.

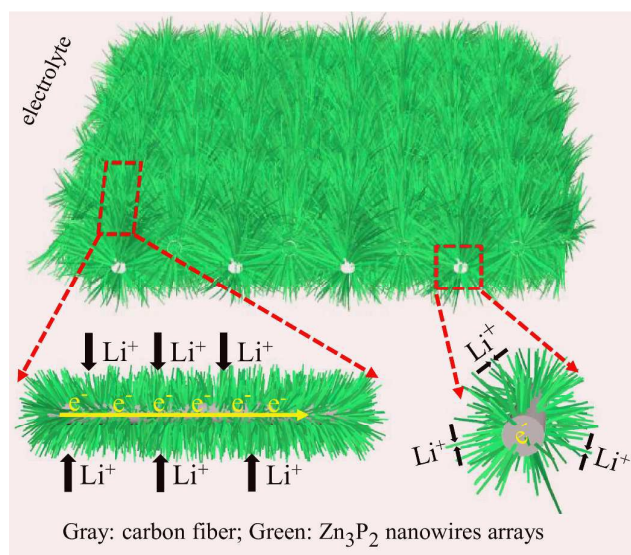


Figure 4. Schematic representation and operating principles of rechargeable lithium-ion battery based on Zn_3P_2 nanowire arrays/carbon cloth.

Prompted by the unique desirable nanoarchitecture, it is expected that the as-prepared integrated Zn_3P_2 nanowire arrays/carbon cloth (IZPNACC) anodes would be advantageous as electrode materials for LIBs. To estimate the lithium-storage reactivity of the as-prepared IZPNACC anodes, the self-supported, binder-free anodes were directly applied to the lab-made CR2032 half cells. Such a design renders no addition of other inactive auxiliary additives in conventional slurry-pasted electrodes like conductive agent and organic insulated binder. This method not only avoids the conventionally complicated electrode preparation process, thus can benefit the mass production but also ensures good electric

conductivity contact and large available lithium-reactivity surface. According to the CV curves (as shown in Figure S1), there are two peaks at ca. 0.6 and 0.15 V in the cathodic scan, which can be attributed to the formation of the Li_3P and LiZn alloys during lithium insertion reaction ($9 \text{Li}^+ + 9 \text{e}^- + \text{Zn}_3\text{P}_2 \rightarrow 3 \text{LiZn} + 2 \text{Li}_3\text{P}$), respectively. Meanwhile, two plateaus at ca. 0.3 and 0.65 V in the anodic scan correspond to the dealloying reaction of LiZn ⁴²⁻⁴⁶ and Li_3P ,⁴⁷⁻⁵⁸ ($3 \text{LiZn} + 2 \text{Li}_3\text{P} \rightarrow 9 \text{Li}^+ + 9 \text{e}^- + 3 \text{Zn} + 2 \text{P}$), respectively. **Figure 3** shows the corresponding lithium-storage measurements of the as-grafted IZPNACC electrodes vs. Li metal at 400 mA g^{-1} at room temperature within the voltage window of 0.01-3 V. **Figure 3a** shows the voltage vs. specific capacity curves of the as-synthesized IZPNACC electrodes for the 1st, 2nd, 10th, 50th, and 190th discharge/charge cycles. We can observe the discharge capacities of the three-dimension hierarchical integrated electrode for the 1st, 2nd, 10th, 50th, and 190th cycle which are evaluated to be about 1350, 1200, 1000, 1020, and 1100 mA h g^{-1} , respectively. And meanwhile, the typical differential capacity-voltage plot is also consistent with the above-mentioned CV curves.⁵⁹⁻⁶⁰ The initial cycle gives the charge capacity of ca. 1185 and thus deliver an initial coulombic efficiency of 88%. Such a high coulombic efficiency can be assigned to the featured merits of the self-supported binder-free architectures as well as the inherent high conductivity and double-lithium-reactivity components characterizations of Zn_3P_2 . Considering such smooth discharge/charge curves, relative low and secure reaction plateau, high initial coulombic efficiency and together with large capacity, the as-formed hierarchical self-supported binder-free IZPNACC anodes are expected to be perfect integrated anode candidate for flexible LIB full cell devices. **Figure 3b** represents the discharge/charge capacities and the corresponding coulombic efficiency vs. cycle number curves of the as-prepared hierarchical self-supported binder-free IZPNACC anodes at 400 mA g^{-1} . The capacity plot (red line) clearly shows that: except for the initial cycle, the subsequent discharge/charge capacities can be well maintained at 1000 mA h g^{-1} as long as 200 cycles without obvious capacity loss. From the corresponding coulombic efficiency profile (blue line), we can see that except for the first cycle (88%), the coulombic efficiency is more than 99% from the 2nd cycle to the 200th cycle. The morphologies (as shown in Figure S2) of the integrated anode after cycling can be preserved basically. And this is another reason for this enhanced electrochemical performance. As for the current collector, it contributes negligible capacity to the integrated anode. As shown in Figure S3, the blank carbon textile fabric shows low capacity (less than 30 mA h g^{-1} and the total capacity contribution of carbon fabric has been excluded when the electrochemical performance of Zn_3P_2 nanowire arrays were evaluated) and the area capacity difference between the integrated anode and the carbon cloth collector at an area current density of $800 \mu\text{A cm}^{-2}$ has also been given in Figure S4. We can see that the area capacity of the integrated anode is as 4.7 times as the pure carbon cloth collector, which indicates main capacity of the integrated anode comes from the lithium-reactive Zn_3P_2 nanowire arrays.

The high-rate capability is an essential part for various LIBs applications, such as hybrid electric vehicles and smart electronics devices. The above-mentioned excellent/inspirational galvanostatic cyclability stimulates us to further investigate the rate capability of the as-formed hierarchical self-supported binder-free IZPNACC anodes within the potential window of 0.01-3 V vs. Li^+/Li . As shown in **Figure 3c**, the rate performances of the as-obtained IZPNACC anode are highly impressive. It can also be clearly observed that the as-formed integrated anode shows excellent capacity retention at different rates. Even at an ultrahigh rate of 15 A g^{-1} , the specific capacity can be still maintained as high as 400 mA h g^{-1} , still higher than the theoretical capacity of graphite (ca. 372 mA h g^{-1}). Large reversible capacities of 1030 mA h g^{-1} at 0.4 A g^{-1} , 850 mA h g^{-1} at 3 A g^{-1} , 700 mA h g^{-1} at 5 A g^{-1} , and 400 mA h g^{-1} at 15 A g^{-1} can be achieved, demonstrating an impressively ultrahigh rate performance of the integrated electrode. Furthermore, a capacity of more than 1010 mA h g^{-1} can be attained once again when the current rate is back to 0.4 A g^{-1} . In addition, from the corresponding coulombic efficiency related to the rate performance plotted in **Figure 3d**, we can also see that the initial coulombic efficiency is consistent with that of the cycle performance showed by the integrated anode. The coulombic efficiency at each current density stage except for the first cycle is also approaching to 99.5%. Such unprecedentedly high-rate performances shown by the as-formed IZPNACC anodes mainly result from the high-speed electron transfer as discussed above and illustrated in **Figure 4**.

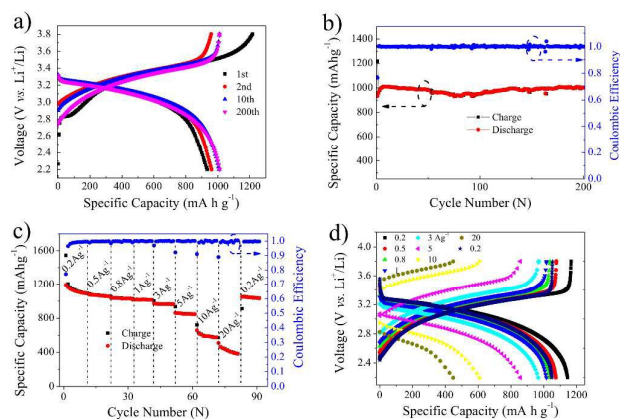


Figure 5. Electrochemical performances of the flexible LIB full cell device with an integrated anode of Zn_3P_2 nanowires arrays/carbon fabric and a cathode of LiFePO_4 microspheres/Al foil, respectively: (a) discharge-charge curves of the full cell at a current density of 400 mA g^{-1} in the voltage range of 2.2-3.8 V; (b) cycle performance and coulombic efficiency of the full cell; (c) rate performance of the full cell at increasing current densities from 0.2 to 20 A g^{-1} ; and (d) the discharge-charge curves of the full cell corresponding to the rate performance.

To validate the practical application in the flexible electronics, we assembled a flexible LIB full cell device by directly using the as-prepared well-aligned IZPNACC electrode as an additive-free anode and commercial LiFePO_4 electrode

(SEM images of the LiFePO_4 electrode are shown in Figure S5) as a cathode. Prior to the full cell test, we first investigated the electrochemical performances of the cathode itself. Figure S6 shows the excellent lithium-storage performances of the cathode including cycle stability, rate performance, etc. The lithium-storage performances of the LIB full cell device (in which the capacity of the cathode is excess to the anode) was explored by charge/discharge in a voltage window of 2.0–3.8 V at 400 mA g^{-1} . Figure 5a shows the charge/discharge voltage vs. capacity curves of the flexible LIB full cell device at the 1st, 2nd, 10th, and 200th cycles, respectively. And the initial coulombic efficiency is 76.7%. These typical charge/discharge curves possess an average discharge voltage plateau of ca. 3.1 V and a charge voltage plateau of ca. 3.5 V, which are well consistent with the CVs results shown in Figure S7. As displayed in Figure 5b, the cycle performances of the flexible full cell device is very stable, with a capacity of ca. 1000 mA h g^{-1} and a coulombic efficiency of ca. 99.5%, demonstrating the high reversibility of the LIB full cell device. The rate performance of the flexible device is also remarkable. As shown in Figure 5c, it can deliver stable capacities of 1100 mA h g^{-1} , 1050 mA h g^{-1} , 1000 mA h g^{-1} , 950 mA h g^{-1} , 850 mA h g^{-1} , 770 mA h g^{-1} , 500 mA h g^{-1} , 300 mA h g^{-1} at varying current rates of 0.2, 0.5, 0.8, 1, 3, 5, 10, 20 A g^{-1} , respectively. When the current rate is reset to 0.2 A g^{-1} , the capacity can easily bounce back to 1070 mA h g^{-1} . Figure 5d depicts the typical discharge/charge curves of the flexible LIB full cell device. The non-stepped discharge/charge curves are favourable to its practical application.

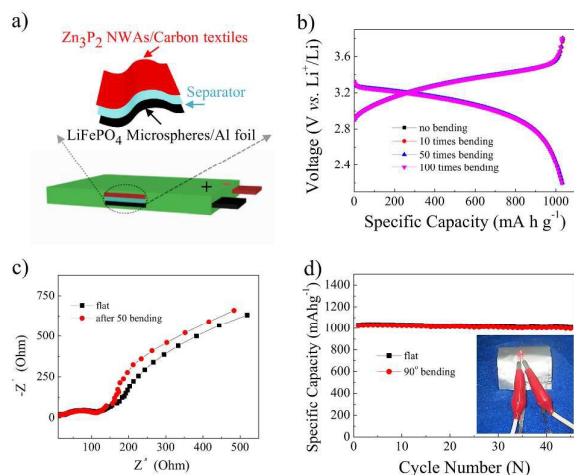


Figure 6. (a) Structure of the flexible LIB full cell device. (b) discharge/charge profiles of the device under the flat and different bending conditions; (c) the nyquist plots of the device carried out at a frequency range from 100 kHz to 0.1 Hz at the flat and 90° bending position; and (d) cycling profiles of the flexible device at a current density of 400 mA g^{-1} up to 45 bending cycles. Inset in panel d: the lighting up of a LED powered by the flexible LIB full cell device based on an integrated anode of Zn_3P_2 nanowires arrays/carbon fabrics and a cathode of LiFePO_4 , respectively.

Figure 6a represents the structure of the flexible LIB full cell. As shown in the inset of Figure 6d, we can see that the flexible LIB full cell device can light up a LED easily under the bending conditions. Furthermore, we tested the voltage vs. specific capacity profiles at varying bending times from 0, 10, 50, to 100 times. The charge/discharge curves at the 0° and 90° bending conditions are almost similar (Figure 6b), suggesting that the bending does not show a negligible effect on the flexible LIB full cell device output voltage. EIS spectra of the fabricated flexible LIB full cell device collected at the flat and bending states are also very similar, which further confirms that bending has little effect on the cell resistance (Figure 6c). The flexible device delivers similar discharge capacities at both flat and 90° bending conditions (Figure 6d). All these results indicate that the novel flexible LIB full cell device by directly using the as-prepared well-aligned IZPNACC electrode as the binder-free anode and the commercial LiFePO_4 as the cathode can exhibit high flexibility, mechanical stability and attractive electrochemical performances. Therefore, the flexible device can be directly applied in various flexible fields, such as bendable/stretchable electronic devices, bendable powering sustainable vehicles, etc.

Conclusion

In summary, we for the first time successfully prepared the self-supported Zn_3P_2 nanowire arrays grafted on carbon fabrics by a facile CVD method. This novel binder-free Zn_3P_2 nanowire arrays/carbon fabric cloth integrated anodes exhibit striking high initial coulombic efficiency, large capacity, excellent rate performance, and long-cycle stability both in coin-type half cells and flexible lithium ion full cells. The largely maintained performances in full cells distinguish this novel anode from most reported anode materials in which an obvious degradation is inevitable for full cells test. Such excellent electrochemical performances can be assigned to the novel well-aligned one-dimensional arrays structure and the synergistic lithium storage of Zn and P components of Zn_3P_2 by forming LiZn and Li_3P . Considering the excellent electrochemical and mechanical properties of this novel anode, there would be a great potential to apply it in future flexible energy storage devices.

Experimental

Synthesis and Characterization of Zn_3P_2

The synthesis was performed by the thermal evaporation of Zn and InP mixed powders. In a typical experiment case, proper amount of Zn and InP bulk were mixed homogeneously by hand and then put the center of a quartz tube. Several round pieces of carbon fabrics were placed downstream at the relative low temperature area (20 cm away from the Zn/P source and the temperature is ca. 300°C). High-purity N_2 gas was acted as a medium at the flow rate of 500 sccm. The furnace was heated up to 800°C and held at the temperature for 2 h. Light yellow powders covered densely on the carbon

fabrics were collected to directly use as integrated anodes for LIB without adding binder and conductive additives. And the loading mass of the Zn_3P_2 in the integrated anode is ca. 3 mg cm^{-2} . The X-ray diffraction data (XRD) were collected from a X-ray diffractometer (X'Pert PRO, PANalytical B.V.) with radiation of a Cu target ($K\alpha$, $\lambda=0.15406 \text{ nm}$) (To avoid the interference of the carbon cloth, the Zn_3P_2 nanowires were scraped from the carbon cloth and transferred onto the Ti foil). The typical morphologies of the integrated anodes were observed by field emission scanning electron microscopy (FESEM, Sirion 200), and transmission electron microscopy (TEM, Philips CM 200).

Electrochemical Measurements

Electrochemical cycling tests were performed with the typical CR2032 coin-type half-cells. The working electrode was prepared by cutting the densely covered Zn_3P_2 nanowire-assembly arrays/carbon cloth into small round pieces for directly using as integrated anodes to perform the electrochemical tests. The electrolyte was 1 M LiPF_6 dissolved in the mixed solvents of ethylene carbonate and diethylene carbonate (volume ratio of EC: DEC = 1:1). And the counter and reference electrodes were both made up of Li foil. The cycle-life of the cells was tested at different rates within a fixed voltage window of $3.0 \text{ V}-0.01 \text{ V}$. The rate capability was estimated by varying the discharge/charge rates from 0.4 A g^{-1} to 15 A g^{-1} . Cyclic voltammetry tests were performed to evaluate the cathodic and anodic reactions within the voltage window $3.0-0.01 \text{ V}$ vs. Li^+/Li with a fixed sweep rate of 0.1 mV s^{-1} . For the flexible LIB full battery, LiFePO_4 on Al foil was served as the counter electrodes and its area (total) capacity is larger (1.2-1.3 times) than that of the Zn_3P_2 anodes and the weight ratio of the cathode and anode materials is ca. 8 to 1. The polymer-aluminum membranes were used to seal the LIB full cell devices and the voltage range was setted within $2.2-3.8 \text{ V}$.

Acknowledgements

We acknowledge the support from Ministry of Science and Technology of China (2015CB932600), National Nature Science Foundation of China (21571073, 51302099, 21322106), Program for New Century Excellent Talents in University (NCET-13-0227), Program for HUST Interdisciplinary Innovation Team and the Fundamental Research Funds for the Central University. We thank the Analytical and Testing Center of Huazhong University of Science and Technology.

Notes and references

- J. Liu, D. Buchholz, R. Chang, A. Facchetti, and T. Marks, *Adv. Mater.*, 2010, **22**, 2333-2337.
- H. Gwon, H. Kim, K. Lee, D. Seo, Y. Park, Y. Lee, B. Ahn, and K. Kang, *Energy Environ. Sci.*, 2011, **4**, 1277-1283.
- L. Li, Z. Wu, S. Yuan, and X. B. Zhang, *Energy Environ. Sci.*, 2014, **7**, 2101-2122.
- Y. Cui, and C. Lieber, *Science*, 2001, **291**, 851-853.

- J. Kim, D. Ko, D. Yoo, D. S. Jung, C. T. Yavuz, N. Kim, I. Choi, J. Y. Song, and J. W. Choi, *Nano Lett.*, 2015, **15**, 2350-2357.
- C. Chan, H. Peng, G. Liu, K. Mcilwrath, X. Zhang, R. Huggins, and Y. Cui, *Nat. Nanotechnol.*, 2008, **3**, 31-35.
- H. Nishide, and K. Oyaizu, *Science*, 2008, **319**, 737-738.
- A. M. Gaikwad, G. L. Whiting, D. A. Steingart, and A. C. Arias, *Adv. Mater.*, 2011, **23**, 3251-3255.
- Z. Chen, J. To, C. Wang, Z. Lu, N. Liu, A. Chortos, L. Pan, F. Wei, Y. Cui, and Z. bao, *Adv. Energy Mater.*, 2014, **4**, 1400207.
- S. Liu, Z. Wang, C. Yu, H. Wu, G. Wang, Q. Dong, J. Qiu, A. Eychmüller, and X. Lou, *Adv. Mater.*, 2013, **25**, 3462-3467.
- C. Guan, X. H. Wang, Q. Zhang, Z. X. Fan, H. Zhang, and H. J. Fan, *Nano Lett.*, 2014, **14**, 4852-4858.
- G. Zhou, D. Wang, P. Hou, W. Li, N. Li, C. Liu, F. Li, and H. Cheng, *J. Mater. Chem.*, 2012, **22**, 17942-17946.
- D. Chao, X. Xia, J. Liu, Z. Fan, C. F. Ng, J. Lin, H. Zhang, Z. Shen, and H. J. Fan, *Adv. Mater.*, 2014, **26**, 5794-5800.
- D. Chao, C. Zhu, X. Xia, J. Liu, X. Zhang, J. Wang, P. Liang, J. Lin, H. Zhang, Z. X. Shen, and H. J. Fan, *Nano Lett.*, 2015, **15**, 565-573.
- J. Song, Z. Yu, M. L. Gordin, S. Hu, R. Yi, D. Tang, T. Walter, M. Regula, D. Choi, X. Li, A. Manivannan, and D. Wang, *Nano Lett.*, 2014, **14**, 6329-6335.
- J. Lee, J. H. Ryu, S. M. Oh, and K. T. Lee, *Adv. Mater.*, 2013, **25**, 3045-3049.
- W. Li, S. Chou, J. Wang, H. Liu, and S. Dou, *Nano Lett.*, 2013, **13**, 5480-5484.
- Y. Zhu, Y. Wen, X. Fan, T. Gao, F. Han, C. Luo, S. Liou, and C. Wang, *ACS Nano*, 2015, **9**, 3254-3264.
- J. Song, Z. Yu, M. L. Gordin, X. Li, H. Peng, and D. Wang, *ACS Nano*, 2015, **9**, 11933-11941.
- X. Fan, J. Mao, Y. Zhu, C. Luo, L. Suo, T. Gao, F. Han, S. Liou, and C. Wang, *Adv. Energy Mater.*, 2015, **5**, 1500174.
- F. Han, T. Gao, Y. Zhu, K. J. Gaskell, and C. Wang, *Adv. Mater.*, 2015, **27**, 3473-3483.
- T. Ramireddy, T. Xing, M. M. Rahman, Y. Chen, Q. Dutercoq, D. Gunzelmann, and A. M. Glushenkov, *J. Mater. Chem. A*, 2015, **3**, 5572-5584.
- W. Li, S. Chou, J. Wang, H. Liu, and S. Dou, *J. Mater. Chem. A*, 2015, DOI: 10.1039/C5TA08590J.
- F. Gillot, L. Monconduit, and M. L. Doublet, *Chem. Mater.*, 2005, **17**, 5817-5823.
- D. C. S. Souza, V. Pralong, A. J. Jacobson, and L. Nazar, *Science*, 2002, **296**, 2012-2015.
- S. Boyanov, J. Bernardi, F. Gillot, L. Dupont, M. Womes, J. M. Tarascon, L. Monconduit, and M. L. Doublet, *Chem. Mater.*, 2006, **18**, 3531-3538.
- W. Li, S. Chou, J. Wang, H. Liu, and S. Dou, *Chem. Commun.*, 2015, **51**, 3682-3685.
- J. Qian, Y. Xiong, Y. Cao, X. Ai, and H. Yang, *Nano Lett.*, 2014, **14**, 1865-1869.
- W. Li, S. Chou, J. Wang, J. H. Kim, H. Liu, and S. Dou, *Adv. Mater.*, 2014, **26**, 4037-4042.
- Y. Kim, Y. Kim, A. Choi, S. Woo, D. Mok, N. Choi, Y. S. Jung, J. H. Ryu, S. M. Oh, and K. T. Lee, *Adv. Mater.*, 2014, **26**, 4139-4144.
- Z. Yu, J. Song, M. L. Gordin, R. Yi, D. Tang, and D. Wang, *Adv. Sci.*, 2015, **2**, 1400020.
- R. Thrinathreddy, T. Xing, M. M. Rahman, Y. Chen, Q. Dutercoq, D. Gunzelmann, and A. M. Glushenkov, *J. Mater. Chem. A*, 2015, **3**, 5572-5584.
- J. Fullenwarth, A. Darwiche, A. Soares, B. Donnadiou, and L. Monconduit, *J. Mater. Chem. A*, 2014, **2**, 2050-2059.
- C. Park, and H. Sohn, *Chem. Mater.*, 2008, **20**, 6319-6324.
- H. wang, M. G. Kim, Y. Kim, S. W. Martin, and J. Cho, *J. Mater. Chem.*, 2007, **17**, 3161-3166.

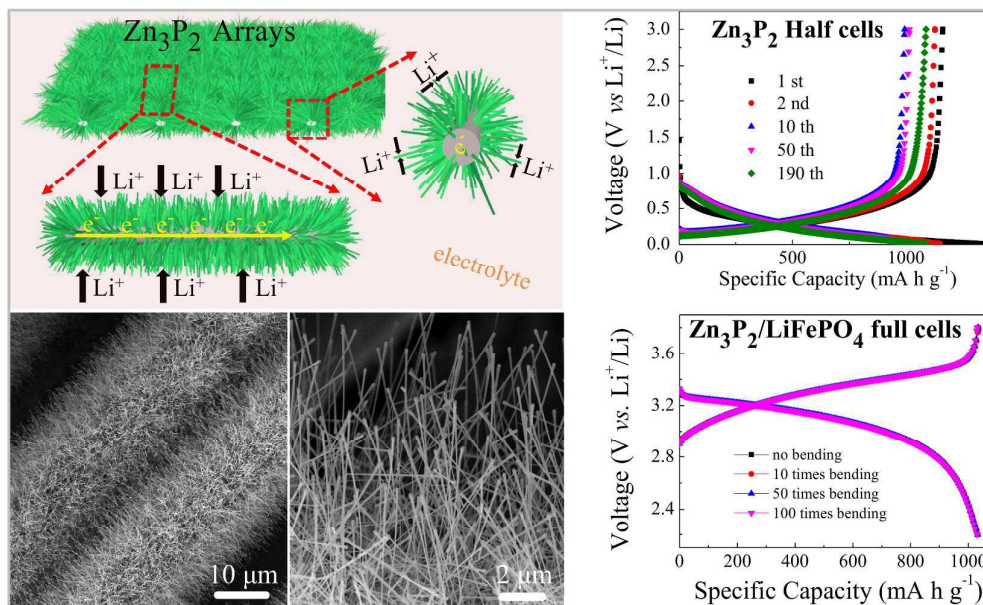
- 36 R. Zou, Z. Zhang, M. Yuen, M. Sun, J. Hu, C. Lee, and W. Zhang, *NPG Asia Mater.*, 2015, **7**, e195.
- 37 R. Elazari, G. Salitra, A. Garsuch, A. Panchenko, and D. Aurbach, *Adv. Mater.*, 2011, **23**, 5641-5644.
- 38 Y. Luo, M. Balogun, W. Qiu, R. Zhao, P. Liu, and Y. Tong, *Chem. Commun.*, 2015, **51**, 13016-13022.
- 39 J. Sun, H. Lee, M. Pasta, H. Yuan, G. Zheng, Y. Sun, Y. Li, and Y. Cui, *Nature Nanotech.*, 2015, **10**, 980-985.
- 40 Y. Luo, J. Luo, J. Jiang, W. Zhou, H. Yang, X. Qi, H. Zhang, H. J. Fan, C. Li, and T. Yu, *Energy Environ. Sci.*, 2012, **5**, 6559-6566.
- 41 W. Ren, C. Wang, L. Lu, D. Li, C. Cheng, and J. Liu, *J. Mater. Chem. A*, 2013, **1**, 13433-13438.
- 42 Y. Hwa, J. Sung, B. Wang, C. Park, and H. Sohn, *J. Mater. Chem.*, 2012, **22**, 12767-12773.
- 43 W. Li, X. Wang, B. Liu, J. Xu, B. Liang, T. Luo, S. Luo, D. Chen, and G. Shen, *Nanoscale*, 2013, **5**, 10291-10299.
- 44 F. Zou, X. Hu, Z. Li, L. Qie, C. Hu, R. Zeng, Y. Jiang, and Y. Huang, *Adv. Mater.*, 2014, **26**, 6622-6628.
- 45 G. Zhang, S. Hou, H. Zhang, W. Zeng, F. Yan, C. C. Li, and H. Duan, *Adv. Mater.*, 2015, **27**, 2400-2405.
- 46 S. Kim, and A. Manthiram, *ACS Appl. Mater. Interfaces*, 2015, **7**, 14801-14807.
- 47 J. Sun, G. Zheng, H. Lee, N. Liu, H. Wang, H. Yao, W. Yang, and Y. Cui, *Nano Lett.*, 2014, **14**, 4573-4580.
- 48 L. Sun, M. Li, K. Sun, S. Yu, R. Wang, and H. Xie, *J. Phys. Chem. C*, 2012, **116**, 14772-14779.
- 49 C. Park, and H. Sohn, *Adv. Mater.*, 2007, **19**, 2465-2468.
- 50 J. Qian, D. Qiao, X. Ai, Y. Cao, and H. Yang, *Chem. Commun.*, 2012, **48**, 8931-8933.
- 51 C. Marino, A. Debenedetti, B. Fraisse, F. Favier, and L. Monconduit, *Electrochem. Commun.*, 2011, **13**, 346-349.
- 52 L. Wang, X. He, J. Li, W. Sun, J. Gao, J. Guo, and C. Jiang, *Angew. Chem. Int. Ed.*, 2012, **51**, 9034-9037.
- 53 M. Bichat, J. Pascal, F. Gillot, and F. Favier, *Chem. Mater.*, 2005, **17**, 6761-6771.
- 54 M. C. López, G. F. Ortiz, and J. L. Tirado, *J. Electrochem. Soc.*, 2012, **159**, A1253.
- 55 Y. Lu, J. Tu, Q. Xiong, J. Xiang, Y. Mai, J. Zhang, Y. Qiao, X. Wang, C. Gu, and S. X. Mao, *Adv. Funct. Mater.*, 2012, **22**, 3927-3935.
- 56 Y. Lu, J. Tu, Q. Xiong, Y. Qiao, J. Zhang, C. Gu, X. Wang, and S. X. Mao, *Chem. Eur. J.*, 2012, **18**, 6031-6038.
- 57 Y. Lu, J. Tu, C. Gu, X. Wang, and S. X. Mao, *J. Mater. Chem.*, 2011, **21**, 17988-17997.
- 58 M. S. Kishore, and U. Varadaraju, *J. Power Sources*, 2005, **144**, 204-207.
- 59 D. Deng, and J. Y. Lee, *Angew. Chem. Int. Ed.*, 2009, **48**, 1660-1663.
- 60 J. Hwang, S. H. Woo, J. Shim, C. Jo, K. T. Lee, and J. Lee, *ACS Nano*, 2013, **7**, 1036-1044.

Self-supported Zn_3P_2 Nanowires Arrays Grafted on Carbon Fabrics as an Advanced Integrated Anode for Flexible Lithium Ion Battery

Wenwu Li,^a Lin Gan,^a Kai Guo,^a Linbo Ke,^a Yaqing Wei,^a Huiqiao Li,^a Guozhen Shen^{*b} and Tianyou Zhai^{*a}

Keywords: Zn_3P_2 nanowire arrays, high-performance, self-supported, flexible, lithium ion batteries

Table of Content



The well-aligned self-supported binder-free **binary lithium-reactive metal phosphide (Zn_3P_2) nanowire arrays** were for the first time successfully grafted on carbon fabrics. When served as integrated electrodes, they exhibit striking high initial coulombic efficiency, large capacity, excellent rate performance, and long-cycle stability **both in coin-type half cells and flexible lithium ion full cells**.